P1.15 OBSERVATIONAL CONSTRAINTS ON CLOUD THERMODYNAMIC PHASE IN MIDLATITUDE STORMS

Catherine M. Naud *
Columbia University, Institute for Space Studies

A. Del Genio
Goddard Institute for Space Studies

1. INTRODUCTION

In order to improve the parameterization of cloud phase transition in general circulation models, aircraft data (Feigelson, 1978; Moss and Johnson, 1994; Bower et al., 1996) have been compiled in different locations and conflicting results emerged. Feigelson (1978) found that mid-level clouds over the former Soviet Union exhibited supercooled droplets down to temperatures as low as -40°C. However, Bower et al. (1996) found that rare were supercooled droplets for temperatures below -15°C in frontal clouds around the British Isles, with the exception of some convective clouds. More recently, ground-based lidar profiles were used to retrieve cloud phase in Southern UK and The Netherlands and found supercooled droplets at cloud top for temperatures down to -30°C (Hogan et al., 2003a, 2003b). GCMs have used these conflicting results to make various choices about the parameterization of cloud phase in stratiform clouds.

More recently, satellite data have been used to retrieve cloud phase information. Doutriaux-Boucher and Quaas (2004) used polarimetric satellite data to evaluate a global lower limit of -32°C for 100% ice fraction, but they did not consider geographic or temporal variations of this quantity, although using the same polarimetric data, Giraud et al. (2001) previously found differences between ocean and land for temperatures of full glaciation. A 10.5-hr spaceborne lidar dataset gave some insights into the global distribution of supercooled droplets at cloud top, and found frequent occurrences in Southern Hemisphere weather systems (Hogan et al, 2004).

* *Corresponding author address:* Catherine M. Naud, Columbia University, Institute for Space studies, 2880 Broadway, New York, NY 10025; e-mail: cnaud@giss.nasa.gov

Aside from temperature, glaciation may also be a function of the vigor of vertical motions and precipitation, depth and age of the cloud, and concentration of ice nuclei. Disagreements among the measurements quoted above may simply reflect sampling of different types of clouds in different locations and dynamic or microphysical conditions.

We proposed to use cloud-top temperature and phase retrievals obtained from the MODerate resolution Imaging Spectroradiometer (MODIS; Salomonson et al., 1989), that is onboard both the NASA-Terra (launched in 1999) and Aqua platforms (launched in 2002). These datasets cover a long period of time (compared to previous studies), and their global coverage allows for a more complete sampling of different atmospheric dynamics and environmental conditions that can affect the temperature dependence of the cloud phase transition. We focus on the oceanic mid-latitude storm tracks, since these are locations of primarily stratiform clouds that exhibit considerable variation in cloud top temperature and phase. The Terra and Aqua MODIS data are collected over the North Atlantic and Pacific winter months (December, January and February), from December 2002 to February 2004. A storm tracking technique is applied to the National Centers for Environmental Prediction - National Center for Atmospheric Research (NCEP-NCAR) reanalysis surface pressures in order to isolate the extra-tropical storm track preferred paths (Bauer and Del Genio, 2006). The complete study is described in Naud et al. (2006), so only the main results are shown here.

2. DATA AND METHODS

2.1 Extra-tropical storm tracks and associated precipitation

Bauer and Del Genio (2006) used NCEP-NCAR reanalysis (Kalnay et al. 1996; Kistler et al.

2001) surface pressures to detect extra-tropical synoptic storms. For the two winters (December, January and February) from December 2002 to February 2004, and each storm in the database, each 6-hour timestep in a storm's lifetime is considered independently and four geographical subsets are constructed according to the location of the pressure minimum at each step. These subsets are: west Atlantic (30°N-60°N; 75°W-50°W), east Atlantic (30°N-60°N; 50°W-0°), west Pacific (30°N-60°N; 150°E-177.5°W) and east Pacific (30°N-60°N; 177.5°W-135°W).

Precipitation rates are obtained from an experimental 3-hourly Tropical Rainfall Measuring Mission (TRMM) combined microwave-infrared dataset (Huffman et al. 2003) for the 6 months selected here. These rates are available globally up to 60° latitude so storms with a low pressure center beyond 60°N were ignored in this study. They are composited for each sub-region defined above using each pressure minimum as the center of a ±25° latitude-longitude grid of 1x1° cells and accumulating the collocated and coincident precipitation rates in each cell. This gives the spatial distribution of precipitation in the area affected by each timestep of a typical storm for each subregion.

Similar composites are also created for the vertical velocity obtained from the NCEP reanalysis. The precipitation rates are used as qualitative indicators of the presence of vertically extended clouds, of areas where glaciation processes may be occurring and are also a means of verifying the validity of the reanalysis vertical velocity fields, i.e., strong precipitation and 500 hPa ascent should generally coincide.

2.2 Cloud properties from MODIS

MODIS is a 36 channels (from 0.4–14.2 μm) imaging spectroradiometer. Cloud products are generated for 5-minute granules of 2030 along-track and 1350 across-track 1-km resolution pixels. Here we used cloud-top temperature and phase to evaluate their relationship at cloud-top. MODIS cloud-top temperatures (of Collection 4) are obtained for 5-km pixels with a CO_2-slicing method for clouds above 700hPa (Menzel et al. 2002) and the 11μm brightness temperatures otherwise. MODIS cloud-top heights were found to have an accuracy of about 1 km with increasing uncertainties as cloud optical thicknesses fall below 0.3 (Naud et al., 2005a,b). Cloud-top phase is estimated from a series of tests involving both visible and near-infrared reflectances and infrared brightness temperatures (see Platnick et al., 2003, for a complete description of the algorithm). A decision tree provides cloud composition at 1 km resolution pixel-level, indicating if a pixel is mainly composed of ice or liquid water. Cloud product generation is fully described in Platnick et al. (2003) and King et al. (2003). In order to match the 1 km resolution of cloud phase with the 5 km resolution cloud-top temperatures, the phase of the central pixel in 5x5 pixel subsets is used. No formal accuracy assessment of the phase retrievals had been conducted at the time of this study. We anticipate that the uncertainty in the phase-temperature relationship is less than the error in either parameter separately, i.e. even if both retrievals fail to refer to the highest cloud in the scene, they are referring to the same cloud.

In addition, each MODIS cloud product granule contains a 5x5 km resolution sea surface temperature (SST) array that is interpolated from the 1°x1° weekly NOAA Optimum Interpolation cloud-free SST dataset (Reynolds and Smith, 1994); this product is also used here.

Figure 1 illustrates the MODIS cloud phase retrieval and associated fields for an East Atlantic synoptic storm observed on 2003-01-19 at a time about 30hr after it was first detected in the reanalysis. Ice is present exclusively at cloud top in the comma-shaped high cloud shield east and north of the surface low in advance of the surface front, but elsewhere liquid water exists at cloud top at various temperatures in different parts of the storm system: 1) In the 500 hPa frontal ascent and precipitation region just east and south of the low, both cloud-top temperature and phase are highly variable on small scales, while cold (< 250 K) liquid water cloud tops occur just west of the low in weak ascent; 2) Along the upward-sloping frontal surface a narrow band of supercooled water exists along the edge of the ice-only high cloud shield; 4) Non-precipitating mid-level water clouds (altostratus or altocumulus) in the 500 hPa descent region west of the low (behind the cold front) are much colder (< 260K) than the low-level liquid water clouds in other descent areas east and north of the front.

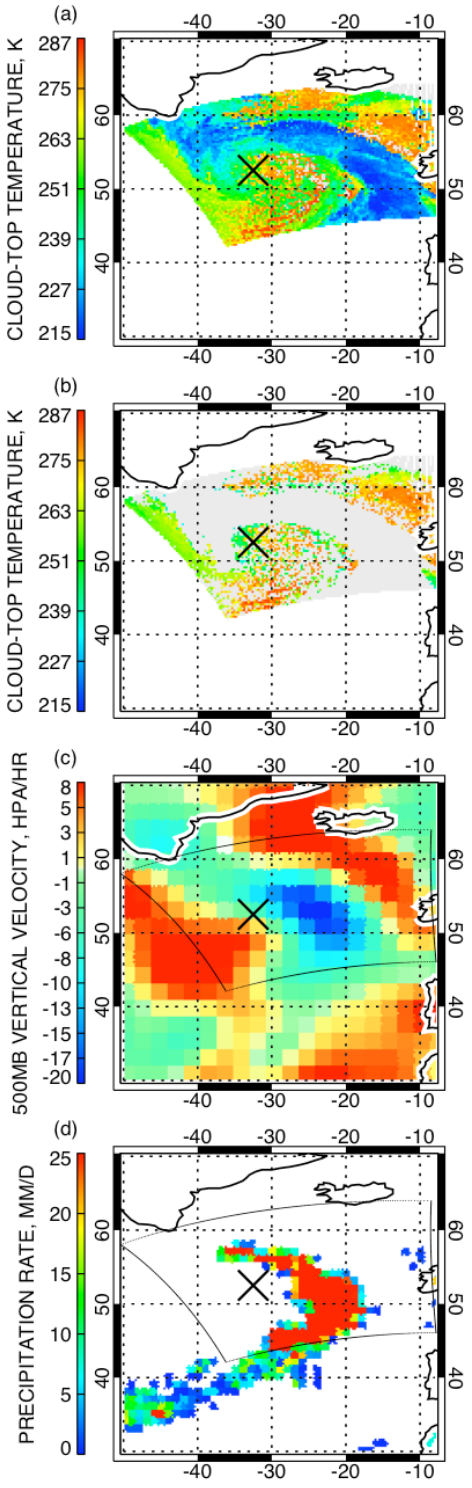

Figure 1: Storm on 01/19/2003 over the Atlantic ocean, 12:00UT, AQUA overpass at 14:30UT, MODIS cloud-top temperature (a), same for only liquid water clouds (b), 500 hPa vertical velocity at 12:00UT (c) and TRMM precipitation rate at 12:00UT (d).

2.3. Data extraction methods

MODIS 5-minute granules obtained from both NASA-Terra (equator crossing local time 10:30) and Aqua (equator crossing local time 13:30) platforms are collected over the North Pacific (30°N-65°N/150°E-135°W) and North Atlantic (30°N-65°N/75°W-0°) oceans for all winter months (December, January and February) from December 2002 to February 2004. A subset is created for which a MODIS granule encompasses a storm pressure minimum within 25° latitude-longitude and 3 hours.

For this subset, the cloud properties are extracted in the following manner: 1) cloud-top temperatures are divided into 2 K bins from 210 to 290K; 2) the number of MODIS 5x5 km water or ice cloud pixels that fall into a 1°x1° cell of a ±25° grid centered on each storm pressure minimum for the 4 sub-regions defined in section 2.1 is estimated for each cloud-top temperature interval; 3) the number of MODIS 5x5 km ice cloud only pixels that fall into the same cell is estimated for each cloud-top temperature interval. For each grid cell, the ice cloud fraction per temperature bin is estimated by dividing the number of ice pixels by the number of ice and water pixels. This is only calculated once all MODIS granules for both winters and all storms have been accumulated. In addition, the cloud-top temperature for exactly 50% ice fraction (T_{50}) is estimated per grid cell, by interpolating the relationship obtained for all temperature bins between ice cloud fraction and cloud-top temperature aggregated over both winters. Consequently, there is a unique value of T_{50} per grid cell. This diagnostic does not imply that phase is only a function of temperature, as we show below; it merely provides a simple way to characterize the statistics of time-mean geographic and synoptic-scale variations in mixed-phase behavior.

In addition, similar composites are created for the median cloud-top temperature (regardless of the cloud phase) and SST.

To unambiguously compare the two ocean basins and the two sides of each storm track, we examine in the next section composites of cloud properties centered on the storm pressure minima for all locations both on and off the nominal tracks.

3. COMPOSITES OF CLOUD AND SURFACE PROPERTIES CENTERED ON STORM SURFACE PRESSURE MINIMA

Synoptic storm composites of 500 hPa pressure vertical velocity for the west and east regions of the Atlantic and Pacific are shown in Figure 2. The composite patterns retain the classic comma structure of baroclinic storms seen in the single-case example of Figure 1, with peak ascent just north and east of the surface low (indicated by the +), a broad (caused by the displacement from one storm and timestep to another) region of ascent east of the low marking the warm front, a second region of ascent extending south and west where the warm sector and cold front occur, and strong descent behind the cold front west of the surface low. In both ocean basins the typical storm is more intense in the western cyclogenesis regions and weakens to the east, more so for Pacific than Atlantic storms. The warm sector – cold front region is broader and extends farther west for Pacific storms than Atlantic storms.

Composites of TRMM precipitation (Figure 3) generally follow the vertical velocity pattern, with cold front precipitation extending ~20° farther west of the surface low in the Pacific than the Atlantic. The one departure from the vertical velocity behavior is that Pacific rainfall in the warm sector decreases less rapidly from west to east than Atlantic rainfall.

The composite SST fields experienced by synoptic storms (Figure 4) are noticeably different for the two ocean basins. In both the Atlantic and Pacific there is a general northwest to southeast SST gradient, maximum near the surface low, and decreasing eastward across both oceans. This is consistent with the general orientation of the storm tracks and the classical understanding of peak cyclogenesis in locations of peak baroclinicity. However, the SST isotherms are more zonal in the Pacific basin. Thus, the different vertical velocity and precipitation composite patterns for the two ocean basins, and specifically the greater westward extent of cold front ascent and precipitation for the Pacific, may be associated with the warmer waters Pacific storms typically encounter southwest of the surface low.

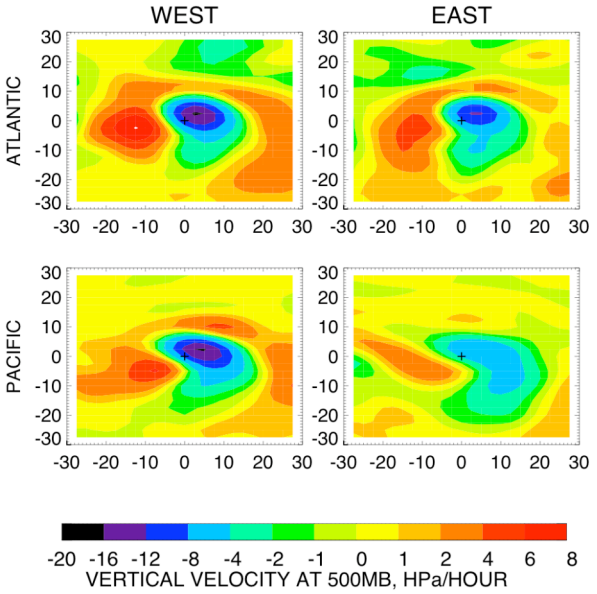

Figure 2: Composites of 500 hPa pressure vertical velocity (negative upward) obtained from the NCEP-NCAR reanalysis for all storm timesteps, over the Atlantic Ocean (top row) west (left) and east (right) of 50°W and the Pacific Ocean (bottom row), west (left) and east (right) of 177.5°W, for all winter months from December 2002 to February 2004. The + indicates the sea level pressure minimum.

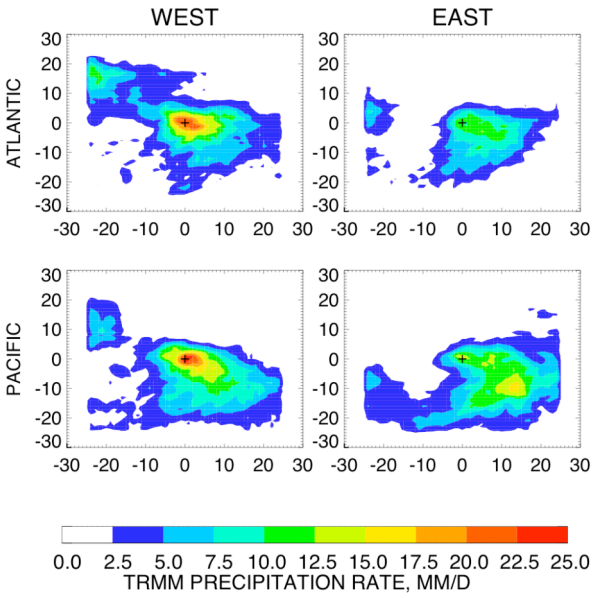

Figure 3: As in Figure 2, but for composites of TRMM precipitation rate.

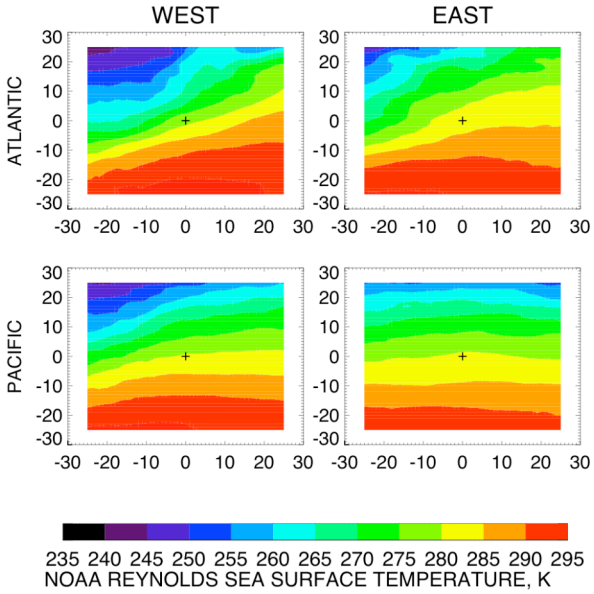

Figure 4: As in Figure 2, but for composites of NOAA Reynolds SST.

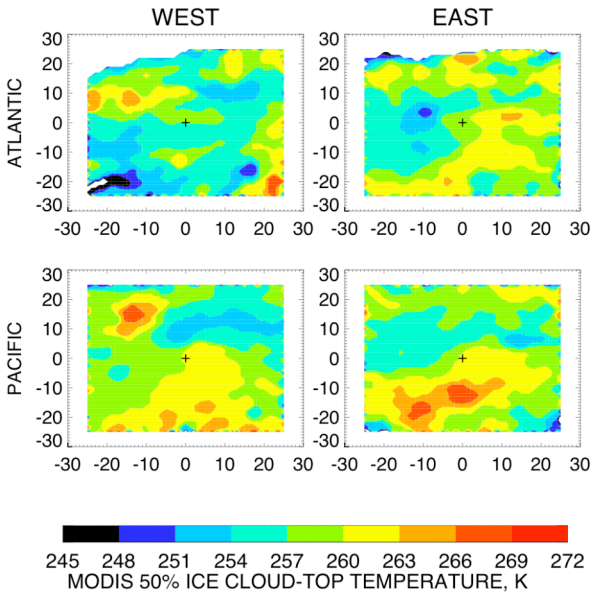

Figure 5: As in Figure 2, but for composites of MODIS T_{50}.

Figure 5 shows the storm composite structure of the T_{50} field. The warmest T_{50} in each subregion is generally in areas of ascent and heavy precipitation, and a more zonally oriented pattern of the warmest T_{50} values occurs in the Pacific than in the Atlantic. T_{50} ~ 260-265 K in these frontal regions, indicating that on average liquid water is restricted to warmer temperatures than in other parts of the storm. Our results at cloud top are similar to observations at various cloud levels by Bower et al. (1996) in similar synoptic situations. Elsewhere, though, supercooled liquid survives to much colder temperatures, with T_{50} ~ 250-255 K. These parts of the storm are generally non-convective and consist of shallower non-precipitating clouds often observed to be liquid at cloud top (Rauber and Tokay 1991; Hogan et al. 2004).

Although warm T_{50} occurs primarily in frontal ascent zones, this association does not directly explain geographic variations in T_{50}. Vertical velocity, precipitation, and SST gradient all decrease from west to east in the frontal regions in both ocean basins (Figure 2 - Figure 4), but ice formation occurs at warmer temperatures moving west to east instead. We discuss how these geographic differences in storm strength may lead to the observed eastward increase in T_{50} in the next section.

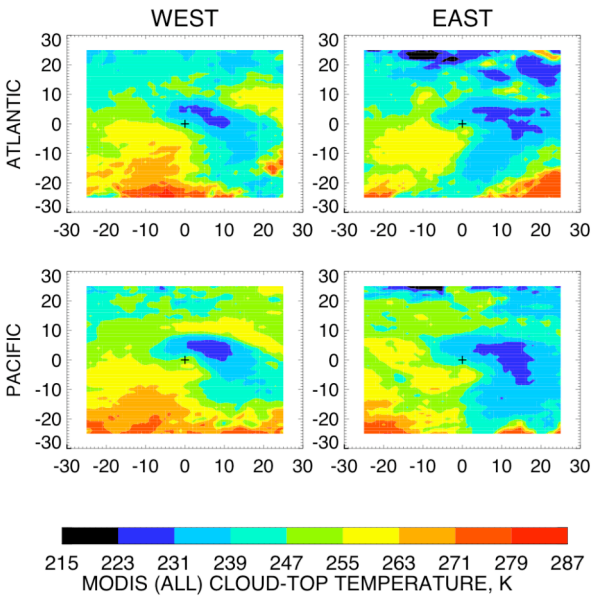

Figure 6: As in Figure 2, but for composites of MODIS cloud-top temperature (for all clouds).

4. DISCUSSION

Other than storm intensity, several other factors that can vary geographically might explain the increase in storm cloud glaciation temperature from west to east.

1) To diagnose whether this might be a signature of the storm lifecycle instead, with glaciation becoming more widespread in the mature stage, we produced composites of T_{50} for

the initial detection, peak sea level pressure tendency, peak intensity (minimum central pressure), and final detection of all storms, regardless of where these occurred geographically. We found no systematic changes from one lifecycle phase to another despite the fact that storm vertical velocities and precipitation are strongest at storm onset and weaken systematically thereafter.

2) We also looked at possible variations in storm depth, i.e., whether ascent to higher altitude in the frontal zone might affect the cloud top temperature dependence of glaciation there. However, the composite cloud top temperature for all clouds (not just those for which ice occurs 50% of the time) is similar in the frontal regions for the western and eastern segments of both ocean basins (Figure 6). Thus, systematic variations in frontal cloud thickness do not seem to exist.

3) Aerosols might also produce geographic differences in glaciation, since the western oceans downwind of Asian and North American pollution sources have higher aerosol loads than the eastern oceans, and the west Pacific more so than the west Atlantic. Mean column aerosol optical depth (observed by MODIS only under clear rather than stormy conditions) is greatest in the southwest sectors of the storm composites, but cloud liquid droplet effective radii retrieved with MODIS (not shown) do not appear systematically different there than elsewhere. This does not rule out the possibility of an aerosol effect on nucleation at higher altitude, but neither is there evidence to suggest that it is a first-order influence.

Thus, we suggest the following picture of processes regulating cloud-top phase as being most consistent with the various composites. In the frontal ascent region of the storm, where the strongest precipitation rates and highest cloud tops occur, glaciation occurs on average at the warmest temperatures. Cloud tops in these regions are at mean temperatures of ~225-240 K (Figure 6), where homogeneous nucleation of the ice phase is common and thus ice exists regardless of the ice nucleus concentration. Thus we only expect MODIS to detect liquid at times and places where cloud top is lower and warmer than the mean value (cf. the region just east of the surface low in Figure 1). However, the very warm T_{50} values in the frontal region suggest other means of glaciating cloud there, e.g., Bergeron-Findeisen growth of ice crystals at the expense of supercooled water droplets (e.g. Pruppacher and Klett, 1978). The significant pixel-level phase variability we sometimes see in frontal zones (Figure 1), the ascent that maintains conditions near water saturation, and T_{50} values close to those at which the Bergeron-Findeisen process operates most efficiently, may indicate the presence of such processes limiting liquid occurrence at colder temperatures.

However, T_{50} (figure 5) is not warm everywhere that the mean cloud-top temperature is coldest (Figure 6), e.g., in the wraparound region north of the surface low and even in the frontal zone of the west Atlantic. In these locations supercooled droplets apparently do not glaciate as readily and instead get lifted to colder temperatures. One possible explanation is the decrease in strength of 500 hPa ascent (Figure 2) from west to east as the SST gradient weakens. Perhaps sufficiently vigorous ascent either suppresses ice formation or advects supercooled liquid water to colder cloud top levels. Bower et al. (1996) suggest that vigorous updrafts in convective clouds do not leave enough time for supercooled droplets to transform into ice crystals in the Hallett-Mossop zone of ice multiplication by graupel – supercooled droplet collisions at warm temperatures (~ 267 K). On the contrary they find larger ice fractions in stratiform frontal clouds observed around the British Isles, where ascent is weaker. Even in the strongest ascent region of our western ocean storms, mean vertical velocities are only ~15 hPa hr^{-1} (~6 cm s^{-1}), well short of typical ice particle fall speeds. However, the strongest ascent regions of storms are the most likely to contain embedded convection, and in a few small-scale regions, updrafts may be strong enough to advect supercooled liquid droplets to cloud top where MODIS detects them. Figure 5 therefore suggests the possibility that the Bower et al. frontal data may be more characteristic of weak storms than intense storms if the east-west differences we observe are indicative of similar differences at deeper levels.

By contrast, outside the frontal zones in both ocean basins, glaciation occurs at consistently colder temperatures at cloud top. Mean cloud tops are warmer (i.e., lower) and precipitation weak in these locations, suggesting a preponderance of shallower midlevel altostratus and altocumulus clouds (cf. Lau and Crane 1995), and vertical velocities are weak or even downward. Thus, the odds of sufficient lifting

taking place for glaciation to occur are reduced. Bower et al. sampled a few such shallow clouds, but perhaps not a sufficient number to be climatologically representative.

Our results help place previous observations of the cloud liquid-ice transition into a large-scale dynamical context. Using the same formalism as Doutriaux-Boucher and Quaas (2004), we find that our MODIS-derived parameter T_{50} would be about 262 K with their dataset, somewhat warmer than our mean value for the two ocean basins of ~258 K in the MODIS data. A colder value of T_{ice} = -38°C (the temperature below which all clouds are ice), especially if combined with a slightly colder assumed temperature below which all clouds are water T_o = -4°C (cf. Del Genio et al. 1996), yields T_{50} ~ -15°C ~ 258 K without changing anything else. Aside from retrieval uncertainties in both datasets, the difference may be due to our focus on midlatitude ocean clouds and the fact that the phase retrieval algorithm in the polarization data is applied only to ~60x60 km overcast regions, which may bias that result toward thicker, more extensive cloud decks.

Comparing our results with Bower et al (1996), we find that the east-Atlantic frontal region exhibits similar temperatures as our composite T_{50} values. However, T_{50} is colder in stratiform clouds outside the frontal region (Figure 5) and in general on the west/north sides of the ocean basins, regions not sampled adequately or at all by Bower et al. Whether the differences we see at cloud top imply similar differences in the interior of clouds is investigated here. For this, we used a 4-year dataset of ground based lidar retrievals of cloud mask (Morille et al., 2006) and cloud phase (Haeffelin et al., 2005a) from the Site Instrumental de Recherche par Teledetection Atmospherique (SIRTA; Haeffelin et al, 2005b), near Paris, France. These retrievals give profiles of cloud ice fraction as a function of time. This instrument is rapidly attenuated in optically thick clouds or when precipitation occurs so only give phase information for non precipitating clouds of less than 3 optical thickness. We used cold months data from November 2002 to March 2006 and constituted a subset for days when a storm was detected in a 25° radius area around the site for the 2002 to 2004 winters. Figure 7 shows the variations in lidar ice cloud fraction as a function of both cloud-top temperature and temperature at the median level within the cloud. Whether looking at times when a storm is nearby or at every winter day, we do not find any significant difference between the cloud's composition behavior at the top or within the cloud. We noticed, however, that T_{50} was much lower than the average quantity for the East Atlantic region. On reason could be that because only thin clouds are sampled, the subset is biased towards clouds similar to the western side of the storm low, where supercooled water persists at cold temperatures. Another hypothesis is that over land, the heavier aerosol load causes droplets to be of smaller size than over the oceans, so their freezing temperature is reduced.

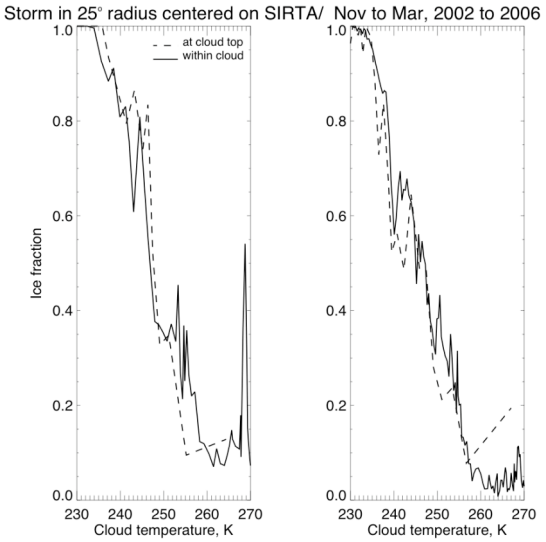

Figure 7: Lidar ice cloud fraction versus cloud-top temperature (dashed) and median cloud height temperature (solid) for winter days with a storm nearby for winters 2002-2004 (left) and all winter days from November 2002 to March 2006.

5. CONCLUSIONS

These results have implications for predictions of cloud feedback and global climate sensitivity, since cloud-radiation interactions are most sensitive to properties near cloud top. Models based on Bower et al. (1996) that do not predict the presence of liquid for T < -15°C may be somewhat biased toward low sensitivity (depending on the degree of difference in parameterized microphysical and radiative properties for liquid vs. ice), because any cloud increase with warming in the mixed-phase zone will overestimate the negative shortwave feedback and underestimate the positive longwave feedback. This was the issue originally raised by Li and Le Treut's (1992) sensitivity tests. Our results do not directly address the ice-liquid

lifetime difference that causes the predicted cloud increase in the models, but any difference between the lifetimes of ice and liquid clouds is reflected indirectly in our occurrence statistics. Thus, parameterizations that misrepresent the processes that control cloud lifetimes should also produce biased ice-liquid occurrence statistics when aggregated over time.

The real message of our study, though, is the need for more physically-based approaches to cloud phase parameterization that allow for different phase behavior in different dynamical settings. The GISS GCM parameterization (Del Genio et al. 1996), for example, allows either ice or liquid to exist in a gridbox at a given timestep. It assumes ice probability at cloud initiation to increase with decreasing T down to -40°C, with saturation relative to the liquid phase in the cloudy part of the box being required to form either phase at these temperatures. However, it takes the additional step of allowing supercooled liquid water that forms to subsequently glaciate if sufficient ice precipitation into a lower supercooled liquid layer occurs. The probability of such glaciation is parameterized to peak at temperatures where Bergeron-Findeisen growth is most efficient. Once the ice phase forms, it remains ice unless particles sediment below the melting level. This should allow for higher T_{50} values in frontal regions, as seen in the MODIS data. In fact, the GISS scheme produces $T_{50} \sim 257$ K over ocean for regions in which the Bergeron-Findeisen process is absent and $T_{50} \sim 264$ K averaged over all ocean regions, in the right direction for synoptic effects but overall somewhat warmer than observed.

More recent cloud parameterizations make no direct assumption about cloud phase, instead carrying ice and liquid water as separate prognostic variables and using microphysical process parameterizations to predict statistics of phase-temperature behavior (cf. Lohmann and Roeckner 1996; Wilson and Ballard 1999; Rotstayn et al. 2000). These schemes are potentially a step forward, but they too have free parameters (e.g., ice nucleus concentration), ambiguity about the spatial relationship between liquid and ice within a gridbox, and uncertainty in how to scale process rates known on the cloud scale to the GCM grid-scale. To date these schemes have been developed using only isolated case studies or limited regional datasets. Even the larger datasets used by Moss and Johnson (1994) and Hogan et al. (2003b) to evaluate existing schemes are climatologically limited spatially (western Europe) and for the former, temporally (11 flights). Our results provide a framework for a more climatically meaningful evaluation that will indicate any potential biases contributing to erroneous cloud feedback estimates.

Acknowledgements. This research was supported by the NASA Radiation Sciences and Precipitation Measurement Missions Programs and the DOE Atmospheric Radiation Measurement Program. The authors are grateful to M. Haeffelin, Y. Morille and V. Noel for providing the SIRTA lidar cloud altitude and phase retrievals.

References

Bauer M. and A. D. Del Genio, 2006: Composite analysis of winter cyclones in a GCM: Influence on climatological humidity. *J. Climate*, **19**, 1652-1672.

Bower, K. N., S. J. Moss, D. W. Johnson, T. W. Choularton, J. Latham, P. R. A. Brown, A. M. Blyth and J. Cardwell, 1996: a parameterization of the ice water content observed in frontal and convective clouds. *Q. J. R. Meteorol. Soc.*, **122**, 1815-1844.

Del Genio, A. D., M.-S. Yao, W. Kovari and K. K.-W. Lo, 1996: A prognostic cloud water parameterization for global climate models. *J. Climate*, **9**, 270-304.

Doutriaux-Boucher, M., and J. Quaas, 2004: Evaluation of cloud thermodynamic phase parameterizations in the LMDZ GCM by using POLDER satellite data. *Geophys. Res. Letters*, **31**, L06126, doi:10.1029/2003GL019095.

Feigelson, E. M., 1978: Preliminary radiation model of a cloudy atmosphere. Part I-Structure of clouds and solar radiation. *Contrib. Atmos. Phys.*, **51**, 203-229.

Giraud, V., O. Thouron, J. Riedi and P. Goloub, 2001: Analysis of direct comparison of cloud top temperature and infrared split window signature against independent retrievals of cloud thermodynamic phase. *Geophys. Res. Lett.*, **28**, 983-986.

Haeffelin, M., Morille, Y. Cadet, B. and V. Noel, 2005a: Lidar techniques to retrieve cloud properties. *In Cloudnet symposium,* Beeskow, Germany 12 Oct 2005. Available from http://www.cloud-net.org/talks/talks.html.

Haeffelin M., and coauthors, 2005b: SIRTA, a ground-based atmospheric observatory for cloud and aerosol research, *Ann. Geophys.*, **23**, 253-275.

Hogan, R. J., P. N. Francis, H. Flentje, A. J. Illingworth, M. Quante and J. Pelon, 2003a: Characteristics of mixed-phase clouds. I: Lidar, radar and aircraft observations from CLARE'98. *Quart. J.Roy. Meteorol. Soc.*, **129**, 2089-2116.

Hogan, R. J., A. J. Illingworth, E. J. O'Connor and J. P. V. Poiares Baptista, 2003b: Characteristics of mixed-phase clouds. II: A climatology from ground-based lidar. *Quart. J. Roy. Meteorol. Soc.*, **129**, 2117-2134.

Hogan, R. J., M. D. Behera, E. J. O'Connor and A. J. Illingworth, 2004: Estimate of the global distribution of stratiform supercooled liquid water clouds using the LITE lidar. *Geophys. Res. Lett.*, **31**, L05106, doi:10.1029/2003GL018977.

Huffman, G. J., R. F. Adler, E. F. Stocker, D. T. Bolvin and E. J. Nelkin, 2003: Analysis of TRMM 3-hourly multi-satellite precipitation estimates computed in both real and post-real time. Combined Preprints CD-ROM, 12th Conf. on Satellite Meteorology and Oceanography, 9-13 Feb. 2003, Long Beach, CA, Amer. Meteor. Soc, 6pp.

Kalnay, E., and co-authors, 1996: The NMC/NCAR 40-year reanalysis project. *Bull. Amer. Meteor. Soc.*, **77**, 437-471.

King, M. D., W. P. Menzel, Y. J. Kaufman, D. Tanré, B. C. Gao, S. Platnick, S. A. Ackerman, L. A. Remer, R. Pincus, and P. A. Hubanks, 2003: Cloud, aerosol and water vapor properties from MODIS. *IEEE Trans. Geosci. Remote Sens.,* **41**, 442-458.

Kistler, R., and co-authors, 2001: The NCEP-NCAR 50-year reanalysis: Monthly means CD-ROM and documentation. *Bull. Amer. Meteor. Soc.*, **82**, 247-267.

Lau, N.-C., and M. W. Crane, 1995: A satellite view of the synoptic-scale organization of cloud properties in midlatitude and tropical circulation systems. *Mon. Weath. Rev.*, **123**, 1984-2006.

Li, Z.-X., and H. Le Treut, 1992: Cloud-radiation feedbacks in a general circulation model and their dependence on cloud modeling assumptions. *Clim. Dyn.*, **7**, 133-139.

Lohmann, U., and E. Roeckner, 1996: Design and performance of a new cloud microphysics scheme developed for the ECHAM general circulation model. *Clim. Dyn.*, **12**, 557-572.

Menzel, P., B. Baum, K. Strabala and R. Frey, 2002: Cloud-top properties and cloud phase algorithm theoretical basis document. *ATBD_MOD_04*, NASA Goddard Space Flight Center. Available on http://modis-atmos.gsfc.nasa.gov/MOD06_L2/atbd.html.

Morille Y., M. Haeffelin, P. Drobinski and J. Pelon, 2006: STRAT : An algorithm to retrieve the STRucture of the ATmosphere from single channel lidar data. Submitted to *J. Atmos. Ocean. Technol.*.

Moss, S. J. and D. W. Johnson, 1994: Aircraft measurements to validate and improve numerical model parameterizations of ice to water ratios in clouds. *Atmos. Res.*, **34**, 1-25.

Naud, C., J.-P. Muller, E. E. Clothiaux, B. A. Baum and W. P. Menzel, 2005a: Intercomparison of multiple years of MODIS, MISR and radar cloud-top heights. *Ann. Geophys.*, **23**, 2415-2424.

Naud, C., J.-P. Muller and P. de Valk, 2005b: On the use of ICESat-GLAS measurements for MODIS and SEVIRI cloud-top height accuracy assessment. *Geophys. Res. Letters,* **32**, L19815, doi:10.1029/2005GL023275.

Naud , C. M., A. Del Genio and M. Bauer, 2006: Observational constraints on cloud thermodynamic phase in midlatitude storms. *J. Climate*, in press.

Platnick. S., M. D. King, S. A. Ackerman, W. P. Menzel, B. A. Baum, J. C. Riédi, and R. A. Frey, 2003: The MODIS cloud products: algorithms and examples from Terra. *IEEE Trans. Geosci. Remote Sens.*, **41**, 459-473.

Pruppacher H. R and J. D. Klett, 1978: *Microphysics of clouds and precipitation*. Kluwer academic, 1st ed., 714pp.

Rauber, R.M., and A. Tokay, 1991: An explanation for the existence of supercooled water at the top of cold clouds. *J. Atmos. Sci.*, **48**, 1005-1023.

Reynolds, R. W., and T. M. Smith, 1994: Improved global sea surface temperature analyses using optimum interpolation. *J. Climate*, **7**, 929-948.

Rotstayn, L. D., B. F. Ryan and J. J. Katzfey, 2000: A scheme for calculation of the liquid fraction in mixed-phase stratiform clouds in large scale models. *Mon. Wea. Rev.*, **128**, 1070-1088.

Salomonson, V. V., W. L. Barnes, P. W. Maymon, H.E. Montgomery and H. Ostrow, 1989: MODIS: Advanced facility instrument for studies of the earth as a system. *IEEE Trans. Geosci. Remote Sens.*, **27**, 145-153.

Wilson, D.R., and S.P. Ballard, 1999: A microphysically based precipitation scheme for the UK Meteorological Office Unified Model. *Q.J.R. Meteorol. Soc.*, **125**, 1607-1636.